Chinese Journal of
POLYMER SCIENCE

RESEARCH ARTICLE

https://doi.org/10.1007/s10118-026-3558-0
Chinese J. Polym. Sci. **2026**, *44*, 1114–1125

Facile Synthesis of an Injectable Redox/pH Dual Stimuli-responsive Hydrogel System for Drug Release

Ning Duan[a,b,†], Xin-Ran Luo[a,b,†], Yan-Di Zhou[a,b], Jun-Yu Chai[a,b], Ji-Zhen Wang[a,b], Jing Gao[a,b], Hui-Fang Ye[a,b], Su-Yan Shan[c,d], Yong Liu[a,b*], and Chang-Chun Yu[a,b*]

[a] *Laboratory of Novel Optoelectronic Technology for Ophthalmic Devices (NOTOD), School of Ophthalmology and Optometry, School of Biomedical Engineering, Wenzhou Medical University, Wenzhou 325027, China*
[b] *National Engineering Research Center of Ophthalmology and Optometry, Eye Hospital, Wenzhou Medical University, Wenzhou 325027, China*
[c] *Department of vitreous and retinal center, Affiliated Eye Hospital of WenZhou Medical University, Hangzhou 310020, China*
[d] *Department of Ophthalmology the First Affiliated Hospital, Zhejiang University School of Medicine, Hangzhou 310003, China*

Abstract Multiresponsive hydrogels, capable of responding to more than one external stimulus, have demonstrated great utility in biomedical applications. This study presents a facile method for preparing an injectable, dual redox/pH-responsive hydrogel system based on poly(3,4-ethylenedioxythiophene):poly(4-styrenesulfonate) (PEDOT:PSS) for the controlled delivery of pharmacologically active bevacizumab (BEV). The hydrogel system was fabricated *via* a one-step physical crosslinking process by mixing PEDOT:PSS with BEV, leveraging electrostatic interactions, hydrogen bonding, and ionic crosslinking. The resulting PEDOT@BEV system exhibited a homogeneously porous structure, robust mechanical stability, and good biocompatibility. Under acidic (pH=5) or alkaline (pH=10) conditions, especially when coupled with elevated reactive oxygen species (ROS) levels, the as-prepared PEDOT@BEV achieved rapid BEV release. This may be attributed to PEDOT oxidation and charge repulsion. In contrast, BEV release remained stable under physiological conditions (pH=7.4, 0 mmol/L H_2O_2). *In vitro* results supported that the resulting PEDOT@BEV demonstrated potent anti-angiogenic efficacy, significantly inhibiting cellular migration and tube formation of human retinal vascular endothelial cells (HRVECs). The vascular endothelial growth factor expression was further reduced. In a mouse model of corneal neovascularization, the PEDOT@BEV system enabled the continuous controlled release of BEV for over 14 days. It exhibited superior anti-angiogenic efficacy compared to free BEV treatment, more effectively reducing neovascularization and corneal inflammation. The designed platform in this work demonstrated versatility by successfully incorporating other therapeutic antibodies (*e.g.*, rituximab, trastuzumab), highlighting its potential for tailored drug delivery in oncology and neovascular diseases. The outcome of this study offers a promising strategy for spatiotemporally controlled drug release in response to specific microenvironmental cues.

Keywords Dual-responsive hydrogel; PEDOT:PSS; Bevacizumab; Anti-angiogenesis; Controlled drug delivery

Citation: Duan, N.; Luo, X. R.; Zhou, Y. D.; Chai, J. Y.; Wang, J. Z.; Gao, J.; Ye, H. F.; Shan, S. Y.; Liu, Y.; Yu, C. C. Facile synthesis of an injectable redox/pH dual stimuli-responsive hydrogel system for drug release. *Chinese J. Polym. Sci.* **2026**, *44*, 1114–1125.

INTRODUCTION

Hydrogels are water-swollen polymer networks with tunable physicochemical properties that are extensively applied in biomedical fields ranging from tissue regeneration to disease therapy.[1] They enable controllable drug release, and possess tunable physical properties, which allow them to protect drugs from degradation and respond to external stimuli.[2]

Stimuli-responsive hydrogels are a specialized subclass capable of undergoing structural and mechanical transformations in response to environmental cues. This kind of hydrogel holds immense promise across diverse pharmaceutical and biomedical applications.[3,4] Their unique ability to dynamically adapt to triggers such as pH,[5] temperature,[6] ionic strength,[7] reduction potential,[8] or their combinations,[9] makes them suitable for controlling drug delivery systems by optimizing drug loading and release, prolonging circulation time, and enabling accurate targeting.

Single-stimuli responsive hydrogels can be limited in therapeutic efficacy since the disease microenvironment is often defined by a combination of multiple factors.[10] The tumor microenvironment, for example, is characterized by an aberrantly low pH arising from an increased metabolic rate and elevated levels of reactive oxygen species (ROS). This is due to the high concentrations of reducing agents, which create a distinct biochemical "fingerprint" that can be exploited for targeted therapy.[11] Dual stimuli-responsive nanocarriers such as those responsive to both pH and redox conditions,[12,13] have been developed to overcome premature drug release at diseased sites and achieve more intelligent delivery.[14] A common design strategy involves incorporating pH-labile chemical bonds (*e.g.*, imine, ester, or amide

* Corresponding authors, E-mail: yongliu@wmu.edu.cn (Y.L.)
E-mail: changchun@wmu.edu.cn (C.C.Y.)
† These authors contributed equally to this work.
Received October 13, 2025; Accepted January 16, 2026; Published online March 3, 2026

bond[5]) and ROS-responsive functional groups (*e.g.*, phenylborate, thioketal, thioether, or ferrocene[15]) into the polymer structure or into polymer/drug conjugates. However, many synthetic methods rely on complex multi-step polymerization processes or chemical conjugation approaches that can compromise pharmaceutical performance.

Poly(3,4-ethylenedioxythiophene):poly(4-styrenesulfonate) (PEDOT:PSS) is a commercial conducting polymer (CP) supplied as an aqueous dispersion of colloidal gel particles. It forms a poly-ion complex *via* electrostatic interactions between $PEDOT^+$ cations and PSS^- anions, where PEDOT molecules aggregate on the PSS chains.[16] Changes in pH can shift bipolarons on the PEDOT chain to polarons by altering the local environment of the PEDOT cations.[17,18] Furthermore, the redox properties of CPs contribute to their sensitivity towards ROS, which is beneficial for drug delivery carriers.[19–21] PEDOT has been used merely as an additive blended into other hydrogel systems as reported elsewhere. This approach can lead to heterogeneous distribution and may limit the responsive performance within the drug delivery system.

In this study, we present a novel single-injection PEDOT hydrogel platform, specifically designed as a carrier for the controlled delivery of bevacizumab (BEV). The hydrogel was facilely synthesized through the physical crosslinking of PEDOT with drugs, while engineered to exhibit simultaneous pH- and ROS-responsive drug release. Both the *in vitro* and *in vivo* profiles of sustained BEV release from the hydrogel were investigated. Additionally, the platform can incorporate other therapeutic antibodies such as trastuzumab (TRZ) and rituximab (RTX), highlighting its potential for tailored drug delivery in the treatment of oncology and neovascular diseases.

EXPERIMENTAL

Materials

PEDOT:PSS was obtained from Agfa-Gevaert N.V. (Shanghai, China). BEV was purchased from Rochester Diagnostics GmbH (Sandhofer, Germany). TRZ was sourced from Shanghai Henlius Biopharmaceutical Co., LTD., (Shanghai, China). RTX was acquired from CHIA TAI Tianqing Pharmaceutical Group Co., Ltd., (Jiangsu, China). Bovine serum albumin (BSA) was obtained from Solarbio (Beijing, China).

Synthesis of PEDOT@BEV Hydrogel

The precursor was prepared by mixing a 0.02 g/mL PEDOT solution with BEV at a volume ratio of 1:1. The mixture was vortexed and left overnight. It was then injected into saline to form the PEDOT@BEV hydrogel. The PEDOT@TRZ and PEDOT@RTX hydrogels were prepared using a similar procedure but with a PEDOT to drug volume ratio of 5:1.

Characterization of Hydrogels

Fourier transform infrared (FTIR)

PEDOT, BEV, and PEDOT@BEV hydrogels were characterized by FTIR using a Nicolet iN10 FTIR spectrometer (Thermo Fisher Scientific, Waltham, MA, USA).

Scanning electron microscopy (SEM)

Hydrogel samples were freeze-dried using a Freeze dryer (ALPHA 2-4 LDPLUS, CHRIST) and sputter-coated with gold. Their morphologies were observed using SEM (Thermo fisher scientific, Waltham, MA, USA) at an accelerating voltage of 15 kV.

Rheological measurement

Hydrogel samples for rheological testing were prepared following the same procedure described above. The precursor solution was vortexed and then allowed to stand for 1, 6, or 12 h. Rheological measurements were carried out at room temperature using a TAAR2000 rheometer equipped with a 40 mm diameter parallel plate. The storage modulus (G') and loss modulus (G'') were measured as a function of angular frequency (0.1–100 rad/s) under a 1% strain.

Cytotoxicity Assay

The cytotoxicity of the hydrogels was assessed by co-culturing with adult retinal pigment epithelial cells (ARPE-19 cell line, Wuhan Pricella Biotechnology Co., Ltd.). Cell viability was evaluated on day 1, 2, and 3 using a Cell Counting Kit-8 (CCK-8, Dojindo, Japan).

Optical density (OD) was measured at 450 nm using a Microplate Reader (Molecular Devices, China), and cell viability was calculated as follows:

$$\text{Cell viability}\,(\%) = \frac{OD_{450hydrogel}}{OD_{450control}} \times 100\% \quad (1)$$

where $OD_{450hydrogel}$ is the absorbance value of the hydrogel group at 450 nm，while $OD_{450control}$ is that of the control group.

In addition, cell viability was determined using Calcein AM/PI fluorescence staining, with live cells emitting green fluorescence and dead cells emitting red fluorescence. To observe the cytoskeletal structure, cells co-cultured with hydrogels for 3 days were stained with rhodamine phalloidin (for F-actin) and DAPI (for nuclei) according to a previous method.[22] Images were captured using an inverted fluorescence microscope (Leica M205FA, Germany). The F-actin content was quantified by measuring the mean fluorescence intensity for each group, with values normalized to the control group.

Scratch Wound Healing Assay

A scratch wound healing assay was performed using human retinal vascular endothelial cells (HRVECs, Shanghai Institutes for Biological Sciences). HRVECs were seeded in 24-well plates at a density of 3×10^4 cells per well and cultured to 100% confluence. Linear scratches were created using a sterile 200 μL pipette tip to generate cell-free gaps. Then, 1 mL serum-free medium containing one of the following was added: 2.5 μL of 0.02 g/mL PEDOT solution, 2.5 μL BEV, or 5 μL PEDOT@BEV hydrogel. 1 mL serum-free medium alone was used as the control group. Wound healing rates were determined at 24 h using an inverted microscope (BX53, Olympus). The images were analyzed using ImageJ software. The cell migration rate was calculated using the following formula:

$$\text{Cell migration rate}\,(\%) = \frac{A_{In\text{-}0h} - A_{W\text{-}24h}}{A_{In\text{-}0h}} \times 100\% \quad (2)$$

where $A_{In\text{-}0h}$ is the initial wound area at 0 h (μm^2), $A_{w\text{-}24h}$ is the wound area at 24 h (μm^2).

HRVECs Tube Formation Assay

HRVECs were seeded at a density of 4×10^4 cells per well onto a layer of 300 μL of matrigel (8.6 mg/mL). After 5 or 10 h of incu-

bation with treatments from the control, PEDOT, BEV, and PEDOT@BEV groups, the degree of tube formation was assessed using an inverted microscope (CKX53, OLYMPUS).

In vitro Drug Release

60 μL of PEDOT@BEV precursor was injected into 5 mL of PBS solution at different pH values (ranging from 5 to 10) containing varying concentrations of H_2O_2 (0, 5, and 10 mmol/L). The concentration of released BEV was measured using a Bicinchoninic Acid kit (BCA-kit, Dalian Meilun Biotechnology Co., Ltd.), and the cumulative drug release percentage was calculated.

Western-blot Assay

ARPE-19 were seeded at a density of 1.5×10^5 cells per well and treated with or without 20 mmol/L H_2O_2 for 24 h. Subsequently, cells were treated with PEDOT@BEV or BEV for another 24 h. Total protein was extracted using RIPA lysate buffer and quantified. Proteins were separated by 10% SDS-PAGE and transferred onto a PVDF membrane (Millipore, MA, USA). VEGF expression was detected using an enhanced chemiluminescent system (Thermo Fisher Scientific, USA). The western blot grayscale values were analyzed using Image J software (Alpha Innotech, San Leandro, USA) for signal intensity.

Animal Study

Establishment of a corneal neovascularization (CNV) model

Male BALB/c mice (2 months old, 20 to 25 g) were purchased from Vital River (Beijing, China). All animal experiments were in compliance with the principles of the Declaration of Helsinki, and were approved by Wenzhou Medical University Animal Experimentation Ethics Committee (Approval Number: wydw2025-0593).

A CNV model was induced by alkali burn, applying 1 mol/L sodium hydroxide to the cornea for 10 s.[23] Alkali-burn mice were randomly divided into 4 groups (n=6 per group). Subconjunctival drug injections were administered on day 1 as follows: CNV group (5 μL of saline), PEDOT group (5 μL of 1% PEDOT hydrogel), BEV group (5 μL of 5 mg/mL BEV solution), and PEDOT@BEV group (5 μL of PEDOT@BEV hydrogel containing 2.5 μL of 2% PEDOT and 2.5 μL of 10 mg/mL BEV solution). Adequate general and local anesthesia was administered before and during all procedures.

Clinical corneal scores

Corneal imaging was performed using a slit-lamp microscope (Carl Zeiss, Jena, Germany) on day 1, 3, 7, and 14 post-treatment. Corneal edema was scored: 0 (absent), 1 (present with visible iris details), 2 (present without visible iris details), and 3 (present without visible pupil). Neovascularization was graded: 0 (none), 1 (vessels in peripheral cornea covering <1/3), 2 (covering <2/3), and 3 (covering >2/3)[24]. Epithelial defects were assessed by fluorescein staining. A 1 μL of 0.1% sodium fluorescein solution (Tianjin Jingming New Technological Development Co., Ltd., Tianjin, China) was applied to each mouse eye. The cornea was examined under cobalt blue light. Images were captured using a slit-lamp microscope. Epithelial defects were scored: 0 (no staining), 0.5 (slight punctate staining), 1.0 (diffuse punctate staining), 2.0 (staining covering <1/3), 3.0 (staining covering 1/3 to 2/3), and 4 (staining covering >2/3). The total clinical corneal score was the sum of the edema, CNV, and epithelial defect scores.

Measurement of corneal thickness

Optical coherence tomography (OCT) was performed on anesthetized mice on day 3, 7, and 14 post-treatment using a CIRRUS HD-OCT 5000 device (Carl Zeiss Meditec, Dublin, CA, USA) to assess corneal structure and thickness. Corneal thickness measurements from OCT images were analyzed using ImageJ software.

Statistical Analysis

Statistical analysis was performed using GraphPad Prism 5 and SPSS 26.0 software. All experiments were analyzed for at least 4 times, and data were presented as mean ± standard deviation (SD). Differences between the two groups were evaluated using the Student's t-test. Differences among three or more groups were assessed by One-way analysis of variance (ANOVA). A p<0.05 was considered statistically significant.

RESULTS AND DISCUSSION

Synthesis and Characterization of PEDOT@BET Hydrogels

The injectable PEDOT hydrogel was formed in a simple process (Fig. 1a), a PEDOT precursor solution, prepared by mixing PEDOT:PSS with BEV, was injected into saline to form the hydrogel. The hydrogel network was established *via* non-covalent interactions, including hydrogen bonding and electrostatic forces. Within the PEDOT:PSS system, the sulfonic acid groups on the PSS chains act as hydrogen bond acceptors for amino groups on BEV, forming intermolecular hydrogen bonds.[25] Furthermore, bivalent ions in the saline solution, such as Ca^{2+}, act as additional ionic crosslinkers by interacting electrostatically with the PSS^- chains.[26]

Additionally, as the isoelectric point of BEV is 7.82–8.70, the protein carriers a net positive charge in physiological environments (pH<7.82).[27] These positive charged regions interact electrostatically with the negatively charged PSS chains, further stabilizing the network through ionic crosslinking.

The drug release mechanism from CPs is primarily driven by changes in the redox state.[28] Under conditions of low pH and elevated levels of ROS, PEDOT undergoes oxidation. During this process, electrons are removed from the PEDOT chains, generating polarons (Fig. 1b). Simultaneously, the incorporation of anions causes the hydrogel to swell. This volume expansion weakens the physical interactions between the hydrogel matrix and the encapsulated drugs, thereby facilitating their release (Fig. 1c).[29]

When the pH increased above 8.7, BEV exists in its anionic form. The interaction between BEV and PSS shifts to repulsion, which promotes drug release. During this process, ion migration within the PEDOT hydrogel is predominantly governed by anions.

During the fabrication process, the concentration of BEV in the precursor played a crucial role. When it reached 50%, Dot-shaped PEDOT@BEV hydrogels with clear outlines were formed when the BEV concentration reached 50% (Fig. 2a). This concentration was therefore selected for all subsequent work, unless otherwise specified. The formed hydrogel displayed a homogeneous and interconnected porous structure (Fig. 2b). The formation of the PEDOT@BEV hydrogel was further confirmed by FTIR analysis (Fig. 2c). The spectrum shows

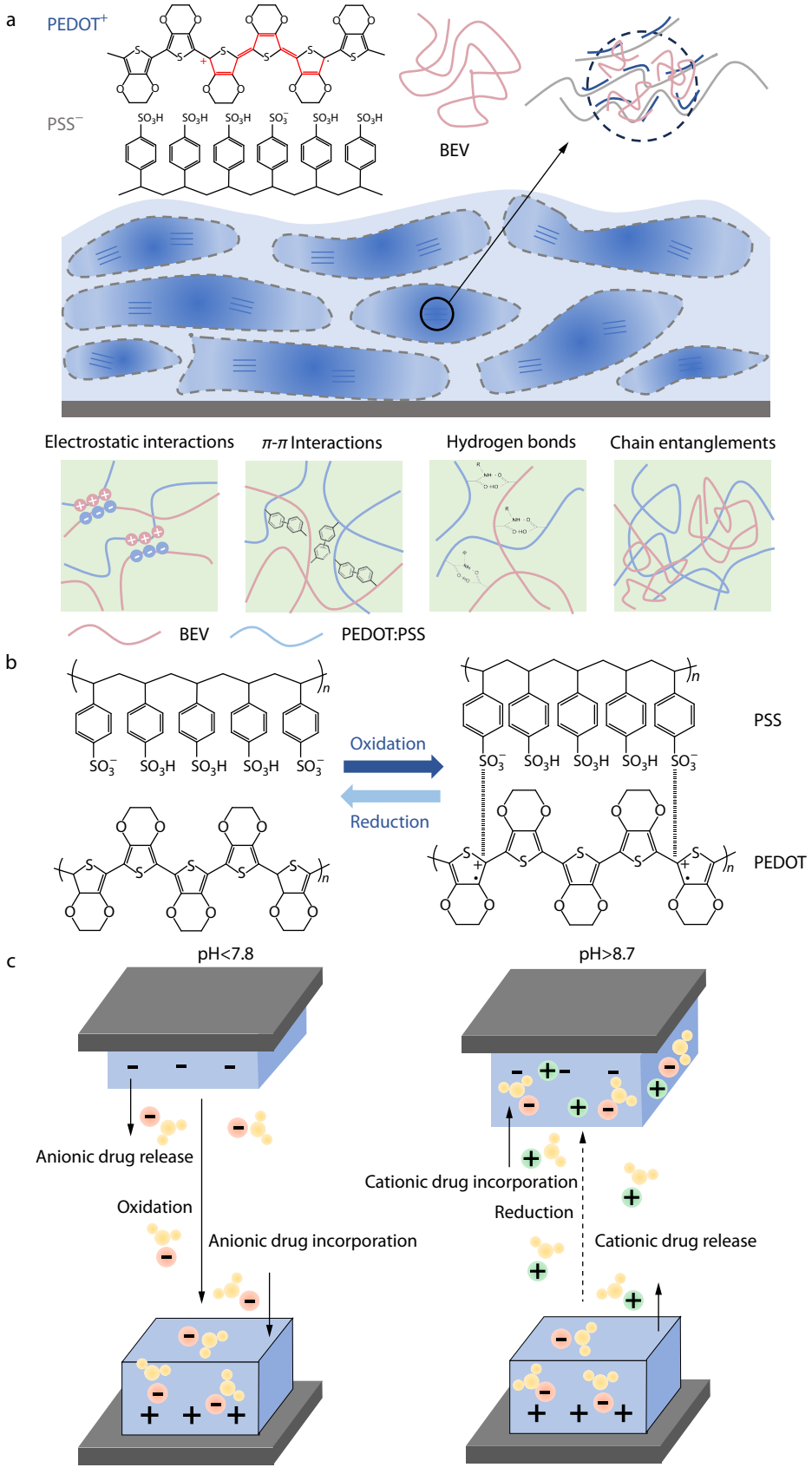

Fig. 1 Principle of PEDOT hydrogel synthesis and drug release mechanisms. (a) Formation procedures of the injectable hydrogel; (b) Redox process of PEDOT; (c) Drug release mechanism of the PEDOT hydrogels under acidic and alkaline conditions.

https://doi.org/10.1007/s10118-026-3558-0

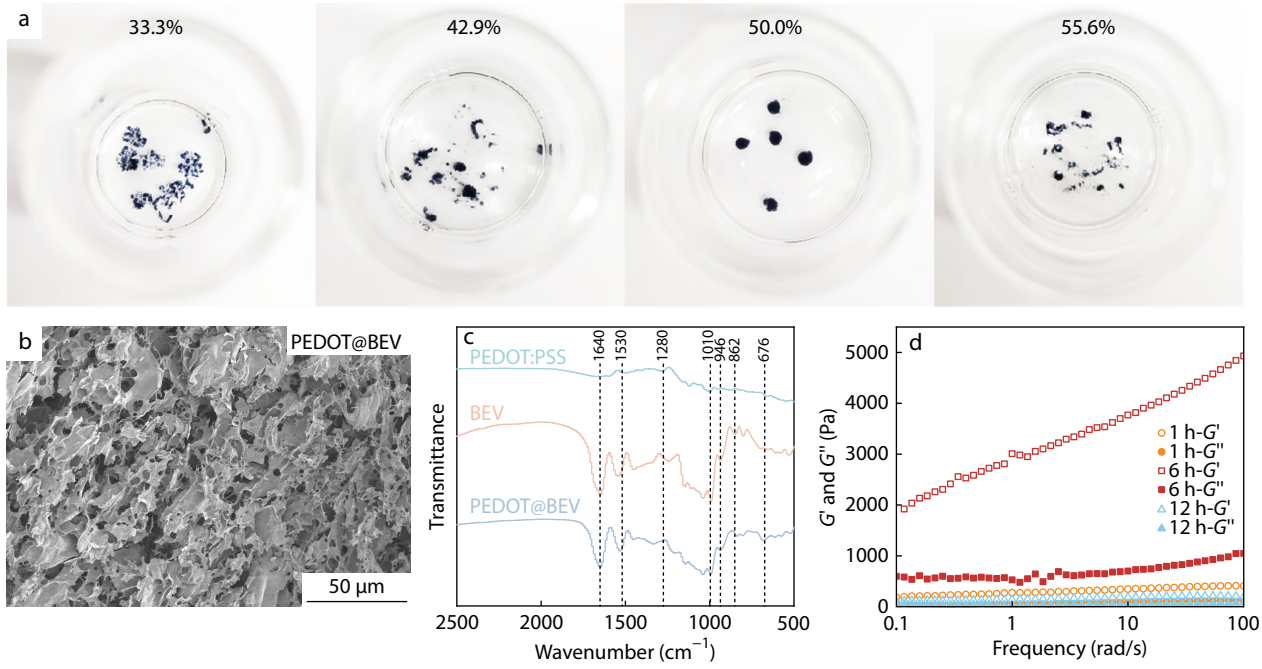

Fig. 2 Characterization of the PEDOT@BEV hydrogel. (a) Digital images of PEDOT hydrogels with varying BEV concentrations; (b) SEM image of the PEDOT@BEV hydrogel; (c) FTIR spectra of PEDOT, BEV, and the PEDOT@BEV hydrogel; (d) Rheological properties of hydrogels with different BEV pre-crosslinking time, where *G'* is the storage modulus and *G"* is loss modulus.

a strong band at 1640 cm^{-1}, attributable to the Amide I vibrations of BEV.[30,31] Characteristic bands of PEDOT can be observed at 1530 and 1280 cm^{-1}, corresponding to C=C and C—C stretching of the thiophene ring, respectively.[32] Absorptions at 946, 862, and 676 cm^{-1} were assigned to C—S bond stretching in the thiophene rings.[33] A band at 1010 cm^{-1} corresponded to the $-SO_3$ group from PSS.[33] These results confirmed the successful formation of the PEDOT@BEV hydrogel. After a 6-h premixing period, the hydrogel exhibits a high plateau storage modulus *G'* between 1.8 and 4.9 kPa (Fig. 2d), which exceeded the loss modulus *G"* (approximately 600 kPa) across the entire frequency range tested. Rheological characterization demonstrated the gel-like behavior of the PEDOT@BEV hydrogel. These results support the excellent mechanical integrity of the PEDOT@BEV hydrogel, a fundamental property that supports its potential application as a drug delivery system.

Cytocompatibility Evaluation of Hydrogel

We then evaluated the cytocompatibility of the PEDOT@BEV hydrogel using a CCK-8 assay. All tested proportions of PEDOT@BEV exhibited good cytocompatibility, with cell viability remaining above 90% cell (Fig. 3a). In addition, cell viability across the four groups (control, PEDOT, BEV, and PEDOT@BEV) remained above 90% throughout the entire experimental period (Fig. 3b). Live/dead staining showed a predominance of viable cells (green) with similar healthy proliferative morphology in all groups on day 1, 2, and 3 (Fig. 3c). Cytoskeleton staining results revealed that ARPE-19 cells adhered and spread well in the presence of the hydrogel, exhibiting a spindle-like morphology comparable to the positive control group (Fig. 3d). The F-actin content in each group was similar to that of the control (Fig. 3e). These results indicate that the prepared PEDOT@BEV hydrogel possesses good biocompatibility as a drug delivery system.

Drug Release from PEDOT@BEV Hydrogels

The release of BEV from PEDOT@BEV hydrogels was investigated across a wide pH range and under various oxidative conditions (Fig. 4a). Under physiological conditions (pH=7.4 and 0 mmol/L H_2O_2), the hydrogel exhibited minimal drug release (Fig. 4b), demonstrating its stability in a normal environment. In contrast, increasing H_2O_2 concentrations triggered drug release, with cumulative release reaching 8.34% at 5 mmol/L and 11.55% at 10 mmol/L by day 14, compared with only 7.68% at 0 mmol/L (Table 1 and Fig. 4c).

The hydrogels also exhibit enhanced release in acidic or alkaline environments. Under mildly acidic condition (pH=6.5, 0 mmol/L H_2O_2, Fig. 4d), the release ratio is low at around 6.07% within the first 4 h and increases moderately to 13.21% over 14 days. When oxidative stress was introduced, release was further promoted, reaching 14.31% (5 mmol/L) and 19.11% (10 mmol/L). Under more severe acidity (pH=5.0, Fig. 4e), drug release was accelerated, reaching 13.84% (0 mmol/L), 17.50% (5 mmol/L), and 19.36% (10 mmol/L), primarily due to oxidation-induced structural changes in PEDOT. Under the alkaline condition (pH=10.0, Fig. 4f), BEV behaves as an anionic drug. Its release significantly enhances by electrostatic repulsion, reaching 28.40% (0 mmol/L), 29.83% (5 mmol/L), and 45.48% (10 mmol/L).

Overall, PEDOT@BEV hydrogels exhibit strong responsiveness to both pH (5.0–10.0) and oxidative stress. Owing to their multi-crosslinked structure and tunable release mechanism, drug release could be finely controlled under diverse conditions. These features highlight the potential of PEDOT@BEV hydrogels as versatile drug carriers for the treatment of tumors and neovascular diseases.

https://doi.org/10.1007/s10118-026-3558-0

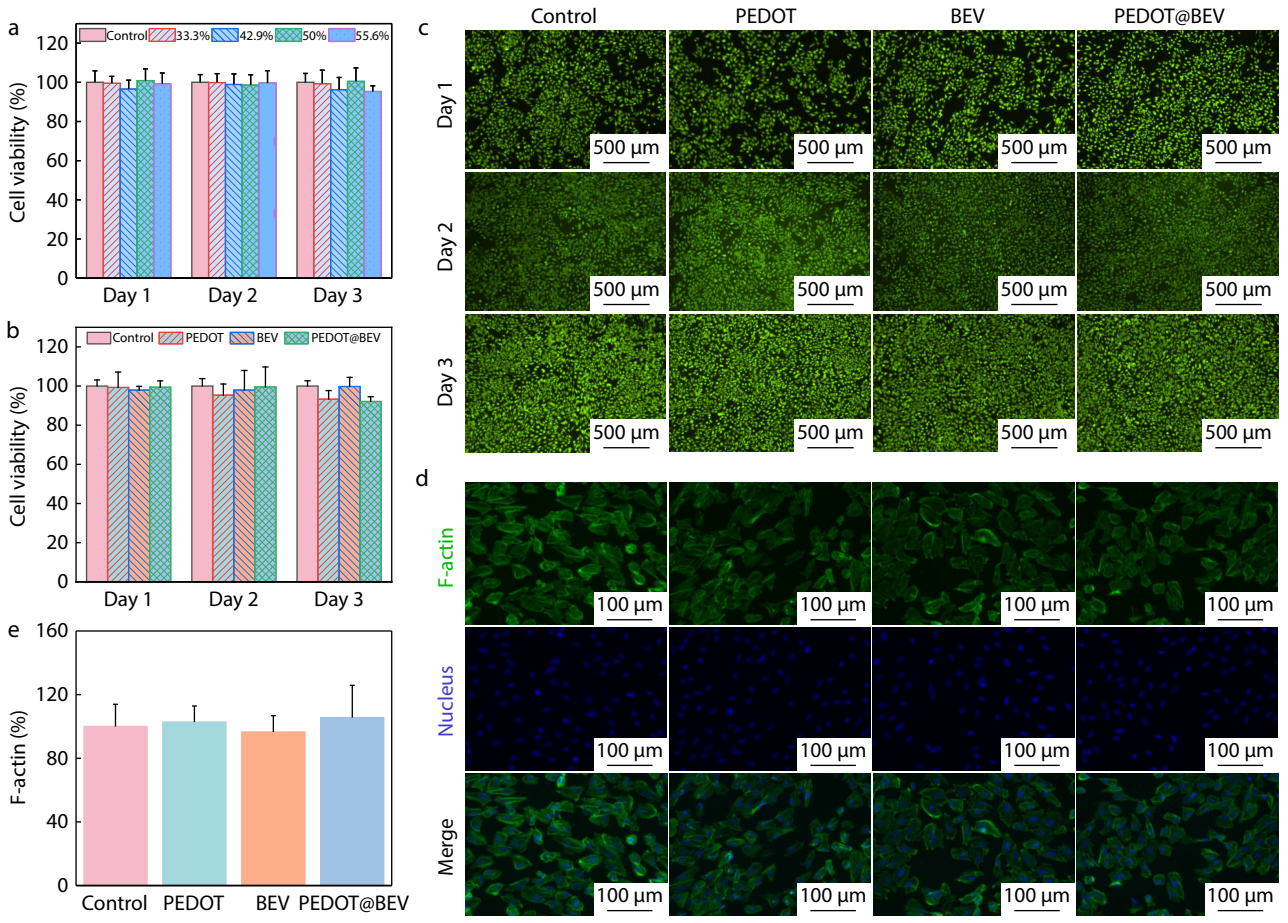

Fig. 3 Biocompatibility of hydrogels. (a) Cell viability of ARPE-19 cells co-cultured with PEDOT@BEV hydrogels at different ratios on day 1, 2, and 3; (b) Cell viability of ARPE-19 cells co-cultured with PEDOT, BEV or PEDOT@BEV hydrogels on day 1, 2, and 3 post-treatment; (c) Live/dead cell staining showing viable (green) and dead (red) cells on day 1, 2, and 3 post-treatment; (d) Fluorescence microscopy images of cells stained for F-actin (rhodamine phalloidin, green) and nuclei (DAPI, blue) on day 3 post-treatment; (e) Quantitative analysis of F-actin content in each group, normalized to the control group.

In vitro Angiogenic Study of PEDOT@BEV Hydrogels

Since BEV is a potent anti-angiogenic drug, the effects of the released BEV from PEDOT@BEV hydrogel on the migration and tube formation of HRVECs were investigated. As shown in Figs. 5(a) and 5(b), both free BEV and PEDOT@BEV treatments significantly inhibit HRVEC migration compares with the control and the pristine PEDOT hydrogel groups. HRVECs are able to form capillary-like structures in Matrigel, serving as an *in vitro* model of angiogenesis. Figs. 5(c) and 5(d) show that abundant tubular networks formed in the untreated control group. In contrast, tube formation was significantly inhibited following treatment with either BEV or PEDOT@BEV. After 5 h, tube formation in the BEV and PEDOT@BEV groups was reduced to 68% and 42% of the control, respectively. The inhibitory effect of PEDOT@BEV became more pronounced after 10 h, with tube formation declining further to 26%. These findings suggest that BEV released from the PEDOT@BEV hydrogel effectively suppresses key angiogenic processes, including migration and tube formation, in

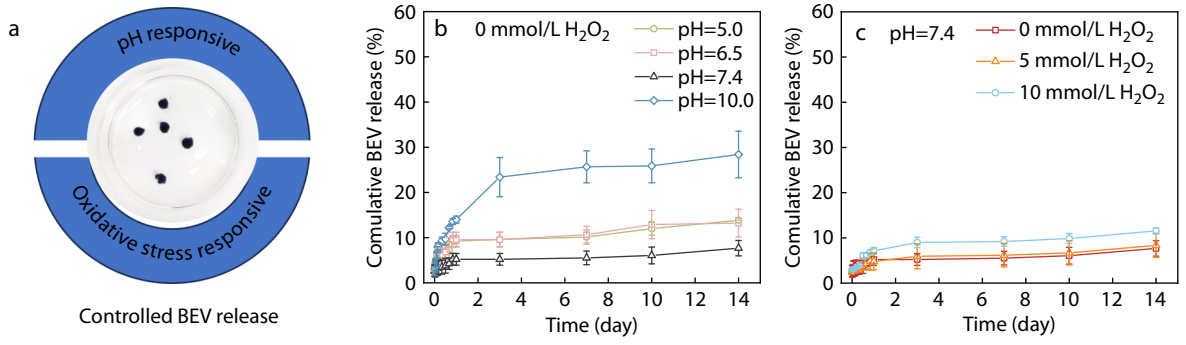

https://doi.org/10.1007/s10118-026-3558-0

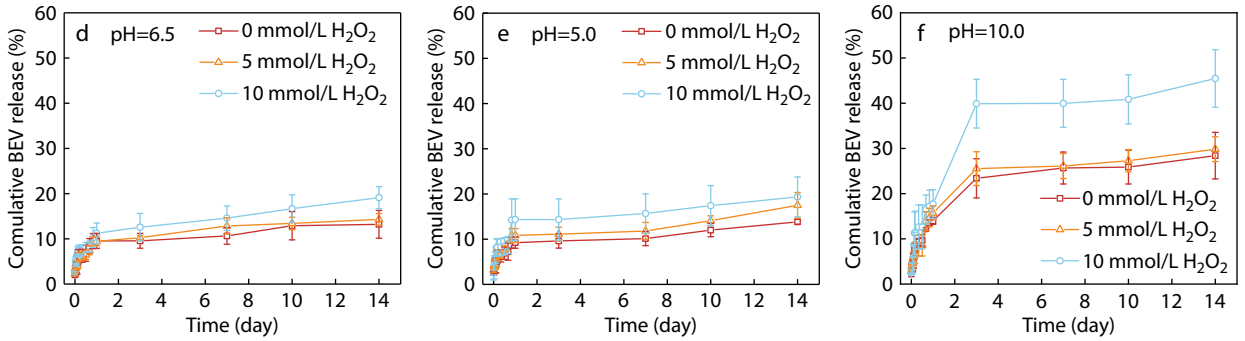

Fig. 4 Drug release profile of PEDOT@BEV. (a) Schematic diagram of drug release; (b) Drug release profile of PEDOT@BEV at 0 mmol/L H_2O_2 over a pH range of 5.0 to 10.0; (c–f) Drug release profiles of PEDOT@BEV at a pH of (c) 7.4, (d) 6.5, (e) 5.0, and (f) 10.0, across a H_2O_2 concentration range of 0–10 mmol/L.

Table 1 Cumulative release of BEV from PEDOT@BEV hydrogel under various conditions after 14 days.

$m_{H_2O_2}$ (mmol/L)	Cumulative release (%)			
	pH=5	pH=6.5	pH=7.4	pH=10
0	13.84%	13.21%	7.68%	28.40%
5	17.50%	14.31%	8.34%	29.83%
10	19.36%	19.11%	11.55%	45.48%

HRVECs *in vitro*.

BEV, a vascular endothelial growth factor (VEGF) inhibitor used to treat various cancers and ocular diseases, functions by specifically binding to VEGF and blocking its activity.[34,35] A western blot assay was performed to confirm that the BEV released from the PEDOT@BEV hydrogel retains its pharmaceutical activity. As shown in Figs. 5(e) and 5(f), elevated VEGF expression under high oxidative stress conditions (20 mmol/L H_2O_2) was confirmed using the western-blot assay. However, treatment with the PEDOT@BEV hydrogel significantly reduced VEGF expression by 54.5%. ($^*p<0.05$). This indicates that the PEDOT@BEV hydrogel effectively decreases the angiogenic capacity of ARPE-19 cells.

Inhibition of Neovascularization by PEDOT@BEV Hydrogels

An alkali-burn CNV model was established to evaluate the *in vivo* efficacy of the PEDOT@BEV hydrogel. As shown in Fig. 6(a), one day after alkali injury, all groups exhibit initial CNV growth accompanied by corneal opacity and edema. Subsequently, CNV continued to progress toward the central cornea in the CNV and PEDOT groups. By contrast, the BEV and PEDOT@BEV groups show decreased vessel growth, indicating effective suppression of neovascularization. Notably, beginning on day 7, the anti-angiogenic effect in the PEDOT@BEV group was significantly stronger than that in the BEV group (Fig. 6b). Corneal opacity and edema, common inflammatory signs associated with CNV progression, can be observed throughout the experiment. Over the 14-day treatment period, the PEDOT@BEV group exhibits milder corneal edema, attributable to its sustained drug release effect. The other 3 groups show similar and more severe edematous responses (Fig. 6c).

In addition, alkali burn-induced corneal epithelial defects were monitored. While healing occurred gradually over 14 days in all groups, the PEDOT@BEV group shows a notably faster repair rate (Figs. 6d and 6e). Composite scores incorporating all three parameters mentioned are summarized in Fig. 6(f). The PEDOT@BEV group achieves the lowest cumulative score. Collectively, these findings demonstrate that the PEDOT@BEV hydrogel functions as a promising drug delivery system for the sustained release of BEV and effectively miti-

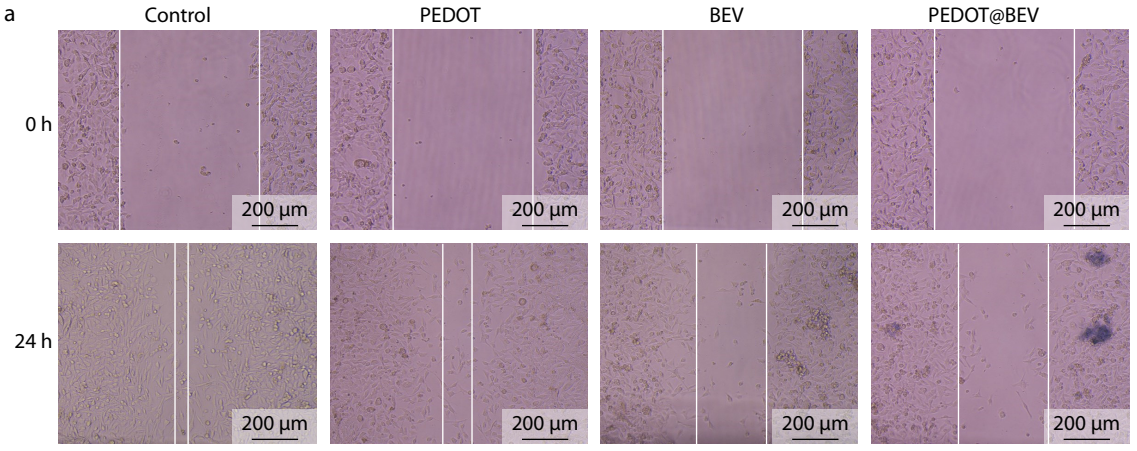

https://doi.org/10.1007/s10118-026-3558-0

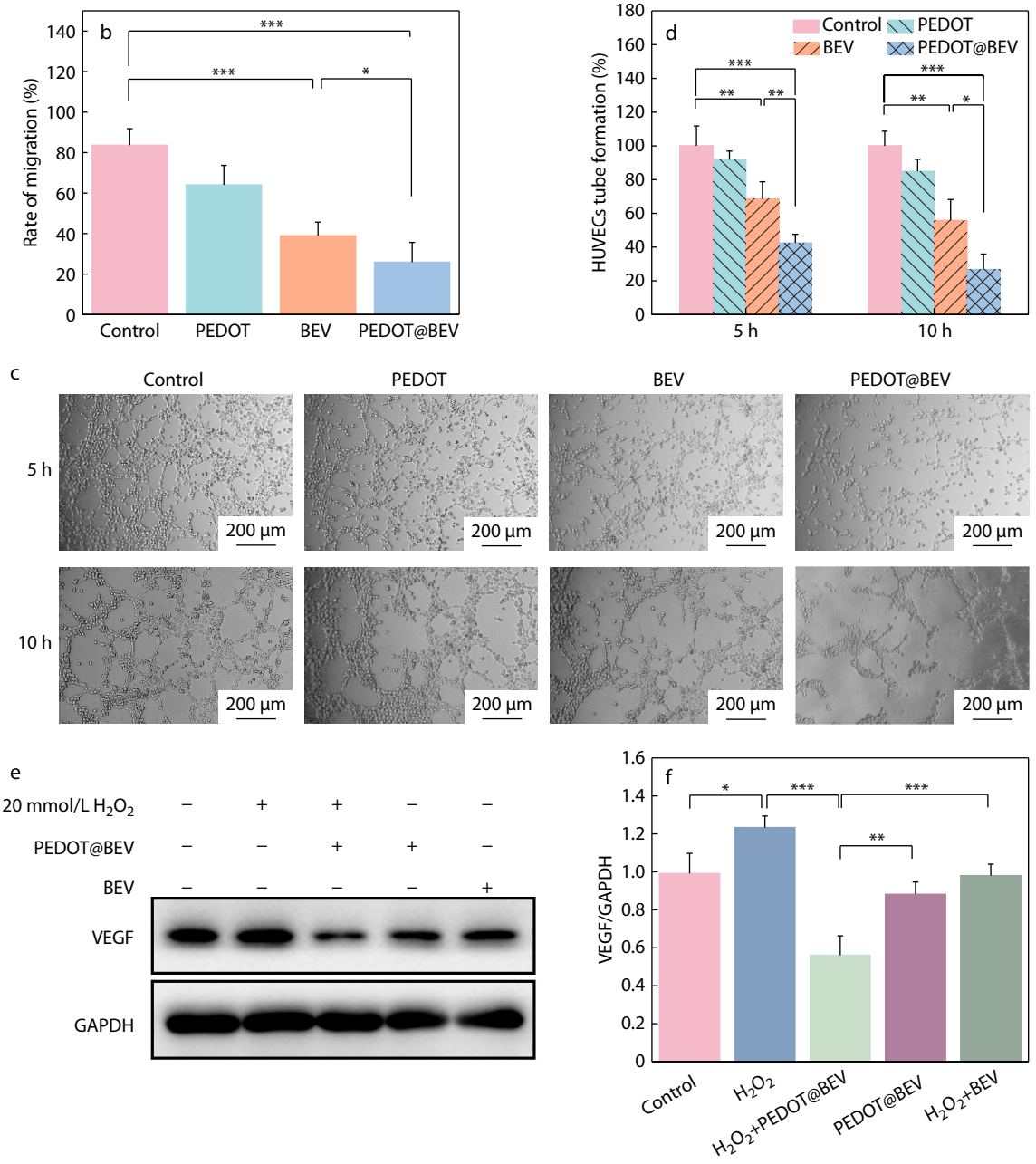

Fig. 5 Anti-angiogenic effects of PEDOT@BEV hydrogels. (a) Representative images of HRVECs wound closure in the four groups (Control, PEDOT, BEV, and PEDOT@BEV) from the cell scratch assay at 0 and 24 h; (b) Statistical analysis of the migration area (%) in the scratch assay (n=6); (c) Tube formation of HRVECs in the different groups after 5 and 10 h; (d) Statistical analysis of the HRVECs tube formation percentage (n=6); (e) Protein levels of VEGF measured by Western-blot analysis; (f) Quantification of VEGF levels by densitometry, normalized to GAPDH (mean ± SD; n=3. $^{*}p$<0.05, $^{**}p$<0.01, $^{***}p$<0.001).

gates CNV progression.

OCT is a powerful imaging technique that enables clear visualization of the anterior segment of the eye, including the cornea, anterior chamber, and iris.[36] Representative OCT images are presented in Fig. 7(a), with quantitative corneal thickness measurements summarized in Fig. 7(b). At 14 days post-treatment, the anterior segment anatomy in the PEDOT@BEV group closely resembled that of the control group. In contrast, abnormal iris folds can be observed in the CNV, PEDOT, and BEV groups. Consistent with these structural observations, corneas in the CNV, PEDOT, and BEV groups exhibited marked thickening attributable to inflammatory edema. By contrast, the increase in corneal thickness was significantly milder in the PEDOT@BEV group.

Extended Applications of PEDOT Hydrogel as Drug Delivery Platform

The developed PEDOT hydrogel platform showed potential as a ROS/pH dual-responsive drug delivery system. Beyond BEV, oth-

https://doi.org/10.1007/s10118-026-3558-0

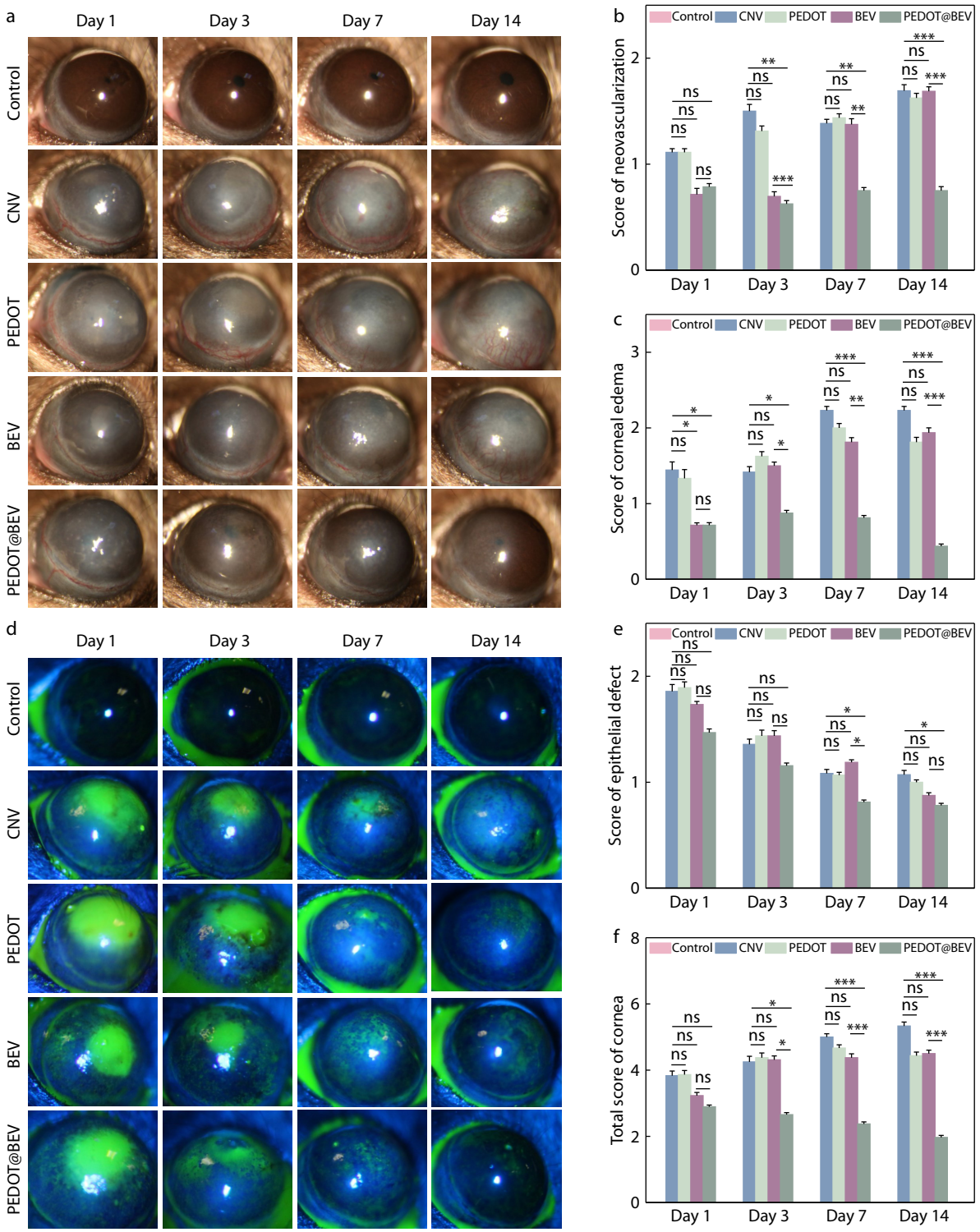

Fig. 6 Anti-angiogenic effects of PEDOT@BEV hydrogels in a CNV model. (a) Representative images of CNV on day 1, 3, 7, and 14 post-treatment; Quantitative scores for (b) CNV area and (c) cornea edema; (d) Representative images of sodium fluorescein staining on day 1, 3, 7, and 14 post-treatment; (e) Scores of corneal epithelial defects; (f) Total composite scores of three indicators above (mean ± SD, n=6 per group, ns: not statistically significant, $^{*}p<0.05$, $^{**}p<0.01$, $^{***}p<0.001$).

er antibody drugs such as RTX and TRZ could also be crosslinked with PEDOT to form the hydrogel (Fig. 8). Both drugs successfully formed three-dimensionally interconnected hydrogels when mixed with PEDOT in a designed ratio, highlighting the broad potential of this approach for controlled drug release in areas such as oncology and immunotherapy.

https://doi.org/10.1007/s10118-026-3558-0

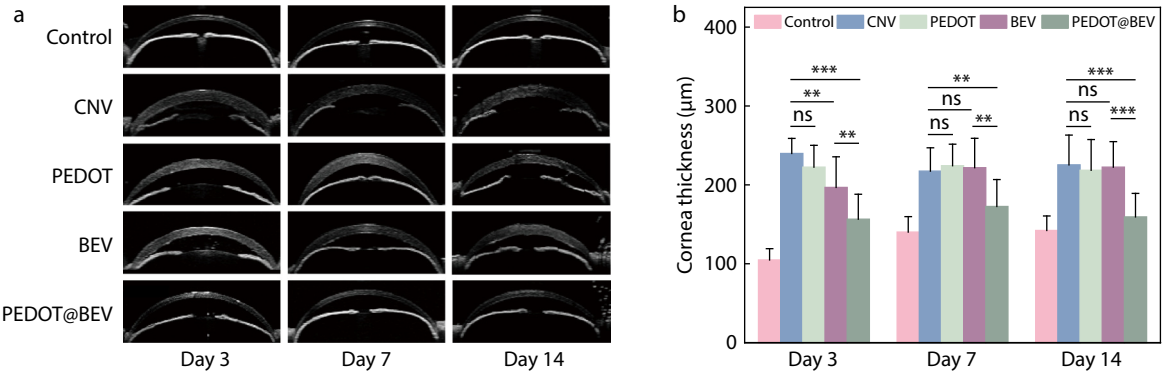

Fig. 7 Cornea thickness on day 3, 7, and 14 post-treatment. (a) Representative OCT images for each group on day 3, 7, and 14 post-treatment; (b) Quantitative cornea thickness in each group on day 3, 7, and 14 post-treatment (mean ± SD, n=6. ns: not statistically significant, $^{*}p$<0.05, $^{**}p$<0.01, $^{***}p$<0.001).

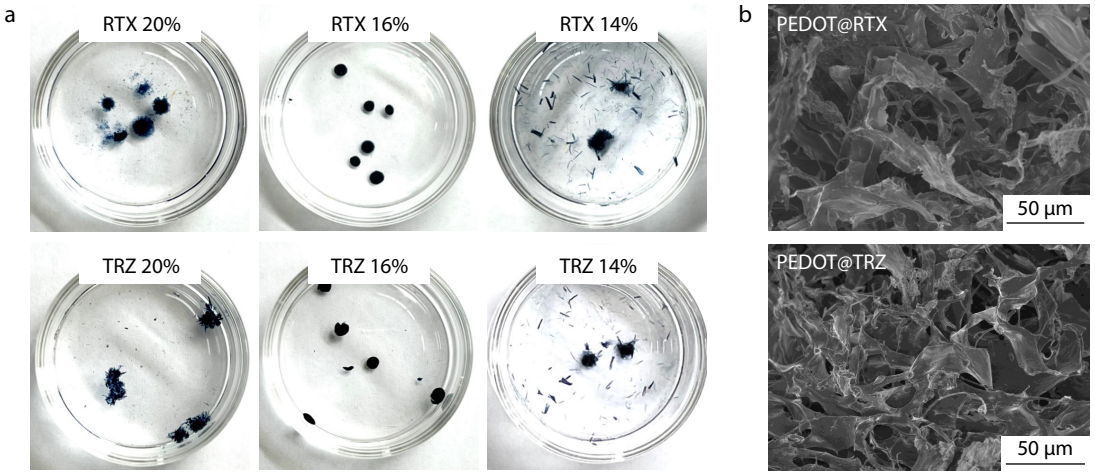

Fig. 8 (a) Digital photographs of PEDOT hydrogels containing varying concentrations of RTX or TRZ; (b) SEM images of the PEDOT@RTX (RTX 16%) and PEDOT@TRZ (TRZ 16%) hydrogels.

CONCLUSIONS

This injectable PEDOT:PSS-based hydrogel platform integrates dual redox and pH responsiveness, enabling precise control over drug release in complex biological environments. The hydrogel was synthesized in a single step through physical crosslinking, which enhances scalability and eliminates the need for complex polymerization. Under acidic or alkaline conditions and elevated ROS levels, the release of BEV was accelerated compared with neutral conditions, accurately reflecting the pathological characteristics of tumor microenvironments. In a mouse CNV model, the PEDOT@BEV hydrogel showed improved controlled release and superior anti-angiogenic effects compared to BEV treatment alone. Moreover, the platform's adaptability to other antibody therapeutics (*e.g.*, rituximab) highlights its broad potential in personalized medicine. Overall, this work advances the development of smart hydrogels for targeted drug delivery, particularly for treating cancers and neovascular disorders characterized by microenvironmental triggers such as low pH and high ROS.

Conflict of Interests

The authors declare no interest conflict.

Data Availability Statement

The data supporting the findings of this study are available from the corresponding author upon reasonable request.

ACKNOWLEDGMENTS

This work was financially supported by the National Natural Science Foundation of China (Nos. 82502583 and U20A20338), Huadong Medicine Joint Funds of Natural Science Foundation of Zhejiang Province (No. LHDMY23H070004), and the Summit Advancement Disciplines of Zhejiang Province (Wenzhou Medical University-Pharmaceutics). We thank Prof. Zou Li (Tsinghua University) for his valuable suggestions. The valuable consultation and instrument supports from Scientific Research Centre of Wenzhou Medical University are also acknowledged.

REFERENCES

1 Cao, H.; Duan, L. X.; Zhang, Y.; Cao, J.; Zhang, K. Current hydrogel advances in physicochemical and biological response-driven biomedical application diversity. *Signal Transduct. Target. Ther.* **2021**, *6*, 426.
2 Li, J.; Mooney, D. J. Designing hydrogels for controlled drug

Graphical Abstract

Facile Synthesis of an Injectable Redox/pH Dual Stimuli-responsive Hydrogel System for Drug Release

Ning Duan, Xin-Ran Luo, Yan-Di Zhou, Jun-Yu Chai, Ji-Zhen Wang, Jing Gao, Hui-Fang Ye, Su-Yan Shan, Yong Liu, and Chang-Chun Yu

Wenzhou Medical University; Affiliated Eye Hospital of WenZhou Medical University; Zhejiang University School of Medicine

An injectable PEDOT@BEV hydrogel with dual redox/pH-responsiveness is developed for smart drug delivery. It shows rapid release under pathological cues of acidic/alkaline pH and ROS while remaining stable physiologically. It is effective in inhibiting angiogenesis *in vitro* and in corneal neovascularization model.

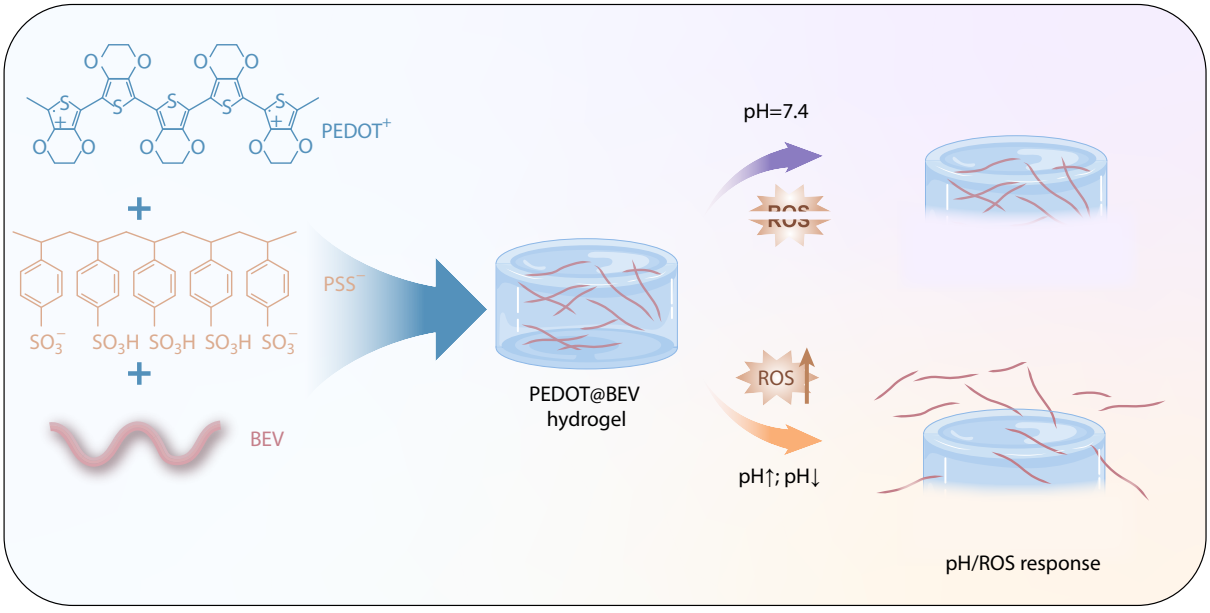

Chinese J. Polym. Sci. 2026, 44, 1114–1125 *https://doi.org/10.1007/s10118-026-3558-0*

delivery. *Nat. Rev. Mater.* **2016**, *1*, 1.
3 Li, Z. Y.; Zhou, Y. Z.; Li, T. Y.; Zhang, J. J.; Tian, H. Stimuli-responsive hydrogels: fabrication and biomedical applications. *View* **2022**, *3*, 20200112.
4 Neumann, M.; di Marco, G.; Iudin, D.; Viola, M.; van Nostrum, C. F.; van Ravensteijn, B. G. P.; Vermonden, T. Stimuli-responsive hydrogels: the dynamic smart biomaterials of tomorrow. *Macromolecules* **2023**, *56*, 8377.
5 Wang, Y. Q.; Dou, X. Y.; Wang, H. F.; Wang, X.; Wu, D. C. Dendrimer-based hydrogels with controlled drug delivery property for tissue adhesion. *Chinese J. Polym. Sci.* **2021**, *39*, 1421–1430.
6 Yu, Y. B.; Cheng, Y.; Tong, J. Y.; Zhang, L.; Wei, Y.; Tian, M. Recent advances in thermo-sensitive hydrogels for drug delivery. *J. Mater. Chem.* **2021**, *9*, 2979.
7 Andrade, F.; Roca-Melendres, M. M.; Durán-Lara, E. F.; Rafael, D.; Schwartz, S. Jr. Stimuli-responsive hydrogels for cancer treatment: the role of pH, light, ionic strength and magnetic field. *Cancers* **2021**, *13*, 1164.
8 Monteiro, P. F.; Travanut, A.; Conte, C.; Alexander, C. Reduction-responsive polymers for drug delivery in cancer therapy—Is there anything new to discover. *Wiley Interdiscip. Rev.: Nanomed. Nanobiotechnol.* **2021**, *13*, e1678.
9 Yang, Z. Y.; Yin, J.; Xin, L.; Li, Y. F.; Huang, Y. J.; Yuan, R.; Zhou, Y. Research advancement of DNA-based intelligent hydrogels: manufacture, characteristics, application of disease diagnosis and treatment. *Chin. Chem. Lett.* **2024**, *35*, 109558.
10 Zhang, J.; Lin, Y. D.; Lin, Z.; Wei, Q.; Qian, J. Q.; Ruan, R. J.; Jiang, X. C.; Hou, L. X.; Song, J. B.; Ding, J. X.; Yang, H. H. Stimuli-responsive nanoparticles for controlled drug delivery in synergistic cancer immunotherapy. *Adv. Sci.* **2022**, *9*, 2103444.
11 Ovais, M.; Mukherjee, S.; Pramanik, A.; Das, D.; Mukherjee, A.; Raza, A.; Chen C. Y. Designing stimuli-responsive upconversion nanoparticles that exploit the tumor microenvironment. *Adv. Mater.* **2020**, *32*, 2000055.
12 Pan, Y. J.; Chen, Y. Y.; Wang, D. R.; Wei, C.; Guo, J.; Lu, D. R.; Chu, C. C.; Wang, C. C. Redox/pH dual stimuli-responsive biodegradable nanohydrogels with varying responses to dithiothreitol and glutathione for controlled drug release. *Biomaterials* **2012**, *33*, 6570.
13 Wang, Z.; Shi, J. J.; Gu, M. Y.; Zhang, X. J.; Sheng, R. L. A versatile strategy to construct surface functionalized pH/redox dual stimuli-responsive nanogels for targeted drug delivery. *J. Appl. Polym. Sci.* **2024**, *141*, e54908.

14 John, J. V.; Uthaman, S.; Augustine, R.; Chen, H.; Park, I. K.; Kim, I. pH/redox dual stimuli-responsive sheddable nanodaisies for efficient intracellular tumour-triggered drug delivery. *J. Mater. Chem. B* **2017**, *5*, 5027.

15 Pu, M. J.; Cao, H.; Zhang, H. J.; Wang, T. Y.; Li, Y. W.; Xiao, S. M.; Gu, Z. P. ROS-responsive hydrogels: from design and additive manufacturing to biomedical applications. *Mater. Horiz.* **2024**, *11*, 3721.

16 Li, Y. C.; Tanigawa, R.; Okuzaki, H. Soft and flexible PEDOT/PSS films for applications to soft actuators. *Smart Mater. Struct.* **2014**, *23*, 074010.

17 Mochizuki, Y.; Horii, T.; Okuzaki, H. Effect of pH on structure and conductivity of PEDOT/PSS. *Trans. Mat. Res. Soc. Japan* **2012**, *37*, 307.

18 de Kok, M. M.; Buechel, M.; Vulto, S. I. E.; van den Weijer, P.; Meulenkamp, E. A.; de Winter, S. H. P. M.; Mank, A. J. G.; Vorstenbosch, H. J. M.; Weijtens, C. H. L.; van Elsbergen, V. Modification of PEDOT:PSS as hole injection layer in polymer LEDs. *Physica Status Solid A.* **2004**, *201*, 1342.

19 Enshaei, H.; Puiggalí-Jou, A.; Saperas, N.; Alemán, C. Conducting polymer nanoparticles for a voltage-controlled release of pharmacological chaperones. *Soft Matter* **2021**, *17*, 3314.

20 García-Fernández, A.; Lozano-Torres, B.; Blandez, J. F.; Monreal-Trigo, J.; Soto, J.; Collazos-Castro, J. E.; Alcañiz, M.; Marcos, M. D.; Sancenón, F.; Martínez-Máñez, R. Electro-responsive films containing voltage responsive gated mesoporous silica nanoparticles grafted onto PEDOT-based conducting polymer. *J. Control. Rel.* **2020**, *323*, 421.

21 He, G. Q.; Li, H.; Liu, J.; Hu, Y. L.; Liu, Y.; Wang, Z. L.; Jiang, P. Recent progress in implantable drug delivery systems. *Adv. Mater.* **2024**, *36*, 2312530.

22 Yuan, F.; Lin, D.; Zhang, Y.; Han, K.; Xu, Q.; Ma, H.; Huang, P. P.; Liu, Y.; Kong, L. D. Nanocomposite from alpha-tocopheryl succinate and chitosan-modified-graphene for efficient inhibition on choroidal melanoma via a chemotherapy-assisted-photothermal therapy. *Chinese J. Polym. Sci.* **2025**, *43*, 1387−1394.

23 Zhu, H. M.; Yu, J. W.; Ye, J. F.; Wu, Y. M.; Pan, J. T.; Li, Y. M.; Chen, C.; Zheng, L.; Liu, G.; Chu, C. C. Nanoparticle-mediated corneal neovascularization treatments: toward new generation of drug delivery systems. *Chin. Chem. Lett.* **2023**, 107648.

24 Li, M.; Chen, Z. F.; Liu, L.; Ma, X. Y.; Zou, J. Topical vitamin C promotes the recovery of corneal alkali burns in mice. *J. Ophthalmol.* **2021**, *2021*, 2406646.

25 Pal, S. C.; Das, M. C. Superprotonic conductivity of MOFs and other crystalline platforms beyond 10^{-1} S cm^{-1}. *Adv. Funct. Mater.* **2021**, *31*, 2101584.

26 Yu, C. C.; Zhou, Y. D.; Yao, S.; Wang, Z. Y.; Ye, S. H.; Qi, R. B.; Hu, H.; Liu, K. K.; Wu, Y. B.; Lawson, T.; Yan, L.; Liu, Y.; Wu, W. W. A facile strategy to restore the optic nerve functionality using an injectable conducting hydrogel. *Adv. Sci.* **2025**, 2415601.

27 Wu, G.; Yu, C. F.; Wang, W. B.; Du, J. L.; Fu, Z. H.; Xu, G. L.; Li, M.; Wang, L. Mass spectrometry-based charge heterogeneity characterization of therapeutic mAbs with imaged capillary isoelectric focusing and ion-exchange chromatography as separation techniques. *Anal. Chem.* **2023**, *95*, 2548.

28 Pang, F. F.; Li, S.; Sun, W. Q.; Han, G. Z. Reversible conductivity modulation of PEDOT:PSS based on pH. *Chem. Phys.* **2017**, *186*, 246.

29 Guimard, N. K.; Gomez, N.; Schmidt, C. E. Conducting polymers in biomedical engineering. *Polym. Sci.* **2007**, *32*, 876.

30 Sousa, F.; Sarmento, B.; Neves-Petersen, M. T. Biophysical study of bevacizumab structure and bioactivity under thermal and pH-stresses. *Acta Pharm. Nord.* **2017**, *105*, 127.

31 Arvinte, T.; Palais, C.; Poirier, E.; Cudd, A.; Rajendran, S.; Brokx, S.; Dowd, J. Part 1: Physicochemical characterization of bevacizumab in undiluted 25 mg/mL drug product solutions: comparison of originator with a biosimilar candidate. *J. Pharm. Biomed. Anal.* **2019**, *175*, 112742.

32 Saini, N.; Lee, D. Y.; Yoon, M. H.; Awasthi, K. Unveiling the potential of Pt nanoparticle-decorated PEDOT:PSS membranes for efficient gas separation. *ACS Appl. Mater. Interfaces.* **2024**, *16*, 7700.

33 Heredia Rivera, U.; Kadian, S.; Nejati, S.; White, J.; Sedaghat, S.; Mutlu, Z.; Rahimi, R. Printed low-cost PEDOT: PSS/PVA polymer composite for radiation sterilization monitoring. *ACS Sens.* **2022**, *7*, 960.

34 Papadopoulos, N.; Martin, J.; Ruan, Q.; Rafique, A.; Rosconi, M. P.; Shi, E.; Pyles, E. A.; Yancopoulos, G. D.; Stahl, N.; Wiegand, S. J. Binding and neutralization of vascular endothelial growth factor (VEGF) and related ligands by VEGF Trap, ranibizumab and bevacizumab. *Angiogenesis* **2012**, *15*, 171.

35 Garcia, J.; Hurwitz, H. I.; Sandler, A. B.; Miles, D.; Coleman, R. L.; Deurloo, R.; Chinot, O. L. *Chinot. Bevacizumab* (Avastin®) in cancer treatment: a review of 15 years of clinical experience and future outlook. *Cancer Treat. Rev.* **2020**, *86*, 102017.

36 Dos Reis, T. F.; de Castro, P. A.; Bastos, R. W.; Pinzan, C. F.; Souza, P. F. N.; Ackloo, S.; Hossain, M. A.; Drewry, D. H.; Alkhazraji, S.; Ibrahim, A. S.; Jo, H.; Lightfoot, J. D.; Adams, E. M.; Fuller, K. K.; deGrado, W. F.; Goldman, G. H. A host defense peptide mimetic, brilacidin, potentiates caspofungin antifungal activity against human pathogenic fungi. *Nat. Commun.* **2023**, *14*, 2052.

https://doi.org/10.1007/s10118-026-3558-0